



Added Value of Chemical Exchange-Dependent Saturation Transfer MRI for the Diagnosis of Dementia

Jang-Hoon Oh¹, Bo Guem Choi², Hak Young Rhee³, Jin San Lee⁴, Kyung Mi Lee⁵, Soonchan Park⁶, Ah Rang Cho⁷, Chang-Woo Ryu⁶, Key Chung Park⁴, Eui Jong Kim⁵, Geon-Ho Jahng⁶

¹Department of Biomedical Science and Technology, Graduate School, Kyung Hee University, Seoul, Korea; ²Department of Biomedical Engineering, Undergraduate School, College of Electronics and Information, Kyung Hee University, Yongin, Korea; Departments of ³Neurology, ⁴Radiology and ⁵Psychiatry, Kyung Hee University Hospital at Gangdong, College of Medicine Kyung Hee University, Seoul, Korea; Departments of ⁶Neurology and ⁷Radiology, Kyung Hee University Hospital, Kyung Hee University, Seoul, Korea

Objective: Chemical exchange-dependent saturation transfer (CEST) MRI is sensitive for detecting solid-like proteins and may detect changes in the levels of mobile proteins and peptides in tissues. The objective of this study was to evaluate the characteristics of chemical exchange proton pools using the CEST MRI technique in patients with dementia.

Materials and Methods: Our institutional review board approved this cross-sectional prospective study and informed consent was obtained from all participants. This study included 41 subjects (19 with dementia and 22 without dementia). Complete CEST data of the brain were obtained using a three-dimensional gradient and spin-echo sequence to map CEST indices, such as amide, amine, hydroxyl, and magnetization transfer ratio asymmetry (MTR_{asym}) values, using six-pool Lorentzian fitting. Statistical analyses of CEST indices were performed to evaluate group comparisons, their correlations with gray matter volume (GMV) and Mini-Mental State Examination (MMSE) scores, and receiver operating characteristic (ROC) curves.

Results: Amine signals (0.029 for non-dementia, 0.046 for dementia, $p = 0.011$ at hippocampus) and MTR_{asym} values at 3 ppm (0.748 for non-dementia, 1.138 for dementia, $p = 0.022$ at hippocampus), and 3.5 ppm (0.463 for non-dementia, 0.875 for dementia, $p = 0.029$ at hippocampus) were significantly higher in the dementia group than in the non-dementia group. Most CEST indices were not significantly correlated with GMV; however, except amide, most indices were significantly correlated with the MMSE scores. The classification power of most CEST indices was lower than that of GMV but adding one of the CEST indices in GMV improved the classification between the subject groups. The largest improvement was seen in the MTR_{asym} values at 2 ppm in the anterior cingulate (area under the ROC curve = 0.981), with a sensitivity of 100 and a specificity of 90.91.

Conclusion: CEST MRI potentially allows noninvasive image alterations in the Alzheimer's disease brain without injecting isotopes for monitoring different disease states and may provide a new imaging biomarker in the future.

Keywords: Chemical exchange saturation transfer; Alzheimer's disease; Lorentzian fitting; Memory correlation; Added value

INTRODUCTION

The neuropathology of Alzheimer's disease (AD) is

generally characterized by the presence of two abnormal proteins in the aggregated state in brain-intracellular neurofibrillary tangles and extracellular amyloid-beta (A β)

Received: May 27, 2020 **Revised:** August 24, 2020 **Accepted:** September 5, 2020

The research was supported by the Basic Science Research Program through the National Research Foundation of Korea (NRF) grant funded by the Korea government (MSIP) (2014R1A2A2A01002728, GHJ), by the Convergence of Conventional Medicine and Traditional Korean Medicine R&D program funded by the Ministry of Health & Welfare through the Korea Health Industry Development Institute (KHIDI) (HI16C2352, GHJ), and by the NRF grants funded by the Korea government (MEST) (No. 2020R1A2C1004749, GHJ).

Corresponding author: Geon-Ho Jahng, PhD, Department of Radiology, Kyung Hee University Hospital at Gangdong, College of Medicine Kyung Hee University, 892 Dongnam-ro, Gangdong-gu, Seoul 05278, Korea.

• E-mail: ghjahng@gmail.com

This is an Open Access article distributed under the terms of the Creative Commons Attribution Non-Commercial License (<https://creativecommons.org/licenses/by-nc/4.0>) which permits unrestricted non-commercial use, distribution, and reproduction in any medium, provided the original work is properly cited.

plaques. Both tau and amyloid proteins are composed of amino acid chains that contain amide, amine, and/or hydroxyl (OH) groups. Neuroimaging is increasingly used to aid the diagnosis of dementia. Structural magnetic resonance imaging (MRI) in patients with AD has shown that progressive atrophy in the hippocampus and loss of whole-brain volume are significantly correlated with the progression of the clinical symptoms of AD. Currently, there is no standard MRI technique that evaluates the alterations in the proteins and neurotransmitters in AD.

Chemical exchange-dependent saturation transfer (CEST) is a new MRI technique that enables the indirect detection of molecules with exchangeable protons [1-3]. The exchange is closely related to the proton concentration and pH in the tissue [4]. Higher proton concentrations result in higher proton transfer values and consequently higher CEST signals. Therefore, this method is sensitive in detecting solid-like proteins and may detect mobile proteins and peptides in tissues [5]. The representative endogenous exchangeable protons are amide, amine, and OH protons. CEST signals are primarily affected by the properties of these biomolecules but are also affected by other factors such as the protein folding state [6] and pH environment [2], which are important markers of many disease processes. A recent animal study showed the possibility of mapping exchangeable protons to monitor protein alterations in the brain of an AD mouse model [7]. A previous human brain study investigated the use of CEST MRI in patients with AD to map amide protons [8]. However, no study has investigated substances such as amide, amine, and OH protons using a full CEST spectrum, also known as the Z-spectrum, in patients with AD. A multi-pool quantification of the full CEST spectrum was introduced using Lorentzian fitting [9-11] and applied in a human brain [10] and a mouse model [11].

In this study, we hypothesized that the CEST MRI technique could sensitively detect changes in proteins and/or metabolites in the AD brain because previous studies showed accumulations of amyloid and tau proteins in patients with AD compared to those in normal subjects. These could be a result of changes in the chemical exchange properties of AD brains. Therefore, the purpose of our study was to evaluate the characteristics of chemical exchange proton pools using the CEST MRI technique in patients with dementia. We investigated amide and amine signals as well as magnetization transfer ratio asymmetry (MTR_{asym}) values at 1, 2, 3, and 3.5 ppm frequency offsets obtained from the

Lorentzian fitting of a full Z-spectrum in subjects with and without dementia.

MATERIALS AND METHODS

Participants

Our institutional review board approved this cross-sectional prospective study, which was performed between March 2015 and December 2018 in our institute (IRB No. khnmc 2015-02-006-001). Informed consent was obtained from all participants. All participants provided a detailed medical history and underwent a neurologic examination, standard neuropsychological testing, and MRI. Cognitive function was assessed using the Seoul Neuropsychological Screening Battery (SNSB) [12], which is included in the Korean version of the Mini-Mental State Examination (K-MMSE) for global cognitive ability. Based on the results of the SNSB examination and MRI findings, this study included patients with mild and probable AD, defined as those with Clinical Dementia Rating scores of 0.5, 1, or 2, according to the criteria of the National Institute of Neurological and Communicative Disorders and Stroke-Alzheimer Disease and Related Disorders Association [12, 13]. These patients were enrolled in the dementia group. Participants with amnesic mild cognitive impairment (MCI) were also included, according to the Petersen criteria [14, 15]. Finally, cognitively normal (CN) elderly participants were selected from among healthy volunteers with no medical history of neurological disease. Both amnesic MCI and CN elderly participants were enrolled in the non-dementia group.

This study included a total of 56 participants. Fifteen participants were excluded from the subsequent analysis for missing CEST MRI scan (1 participant), MMSE scores < 25 (6 CN and 3 MCI participants), MMSE score > 25 (4 AD participants), and lack of full SNSB exam (1 participant). Therefore, of the 41 remaining participants, 19 were allocated to the dementia group (mean = 77.9 years, range = 55–92 years) and 22 were allocated to the non-dementia group (mean = 66.7 years, range = 51–83 years). All 19 dementia participants had AD. In the non-dementia group, 13 participants had CN, while nine participants had amnesic MCI. Table 1 summarizes the demographic characteristics and results of the neuropsychological tests.

MRI Acquisition

Full CEST spectrum data in the brain were acquired using

a three-dimensional (3D) gradient and spin-echo (GRASE) sequence [16] with a 32-channel sensitivity-encoding (SENSE) array coil. We used the following parameters to induce the saturation exchange transfer of protons: B1 amplitude of the saturation pulse of 2 μ T, saturation pulse duration of 200 ms with a 10 ms interval between pulses, and four saturation pulses. The total saturation time was 0.84 seconds. We obtained the full Z-spectrum by a total of 38 dynamics from -5.00 to 5.00 ppm frequency offset ranges using an alternative increased frequency interval. The first acquired image was the reference image S_0 at -40 ppm and the second acquired image was at a 0 ppm offset to direct the saturation of water. The scan time was 9 minutes 27 seconds.

For image registration and brain tissue segmentation, sagittal structural 3D T1-weighted (T1W) images were acquired with the turbo field echo sequence, which is similar to the magnetization-prepared rapid acquisition of the gradient echo (MPRAGE) sequence. In addition, T2-weighted turbo-spin-echo and fluid-attenuated inversion recovery images were acquired to evaluate any brain abnormalities. MRI was performed using a 3T MRI system (Ingenia, Philips Medical System).

Lorentzian Fitting of Full Z-Spectrum Images with Special Frequency Offset Protons

The signals of the full Z-spectrum images were normalized

Table 1. Demographic Data, the Neuropsychological Test Results, and the Segmented Brain Tissue Volumes

	Non-Dementia	Dementia	P
Number of subjects	22 (13 CN, 9 MCI)	19 (AD)	N/A
Age* (years)	66.68 \pm 7.07	77.89 \pm 8.04	< 0.001
Sex [†] (M/F)	6/16	4/15	0.190
K-MMSE*	28.55 \pm 0.91	16.95 \pm 5.22	< 0.001
CDR (range)	0.33 (0-0.5)	1.28 (0.5-2)	N/A
TIV [‡]	1484.95 \pm 119.33	1415.26 \pm 106.58	0.057
TGMV [‡]	601.09 \pm 51.41	509.52 \pm 46.73	< 0.001
TWMV [‡]	484.52 \pm 51.20	415.84 \pm 50.35	< 0.001
TCSFV [‡]	399.90 \pm 57.08	490.39 \pm 58.82	< 0.001

All continuous variables, age, K-MMSE, TIV, TGMV, TWMV, and TCSFV, are presented as mean \pm SD. *Age and MMSE score were compared between two groups by Mann-Whitney test, [†]Gender was compared between the two groups by chi-square test, [‡]TIV, TGMV, TWMV, and TCSFV were compared between two groups by independent *t* test. AD = Alzheimer's disease, CDR = Clinical Dementia Rating score, CN = cognitively normal, K-MMSE = Korean version of Mini-Mental State Examination, MCI = mild cognitive impairment, TCSFV = total cerebrospinal fluid volume, TGMV = total gray matter volume, TIV = total intracranial volume, TWMV = total white matter volume

to the signals of the non-saturated reference image S_0 obtained at a -40 ppm frequency offset. The normalized full Z-spectrum signals (in ppm) were divided into 1280 points in 1 Hz units by interpolation. Voxel-based B0 correction was performed using the 10th polynomial fitting method [17]. The water resonance frequency was estimated as the frequency with the lowest signal intensity from the fitted curve and shifted along the direction of the offset axis to 0 ppm at its lowest intensity. The following six-pool Lorentzian formula was used to obtain the baseline, amplitude, and frequency offset for each of the six pools [9, 18].

$$Z = Z_{ini} = \sum_{i=1}^6 \frac{A_i \cdot \Gamma_i^2 / 5}{\Gamma_i^2 / 5 + (\Delta\omega_{RF} - \delta\omega_i)} \quad (1)$$

where Z_{ini} is the baseline of the six pools, A_i is the amplitude of the six pools, Γ_i is the full width at half-maximum of the six pools, $\Delta\omega_{RF}$ is the radiofrequency, and $\delta\omega_i$ is the frequency offset of the six pools. The initial definitions of the initial values and the low and upper limits (Supplementary Table 1, Supplementary Fig. 1) were as recommended as described previously [9, 18]. The amplitude of the water protons was initially set at the highest value (0.45), while the amplitudes of the amine and amide protons were initially set as equal (0.06). The lower and upper values were defined to minimize mobility with the fitting Z-spectra limitation of the six pools. Finally, the voxel-based MTR_{asym} maps were calculated at frequency offsets of 1.00 (OH), 2.00 (guanidino), 3.00 (amine), and 3.50 (amide) ppm using the following equation [17, 19, 20].

$$MTR_{asym} = \frac{S_{sat}(-\Delta\omega) - S_{sat}(\Delta\omega)}{S_0} \quad (2)$$

where $S_{sat}(\pm \Delta\omega)$ is the saturated transfer signal obtained at a $\pm \Delta\omega$ frequency offset and S_0 is the non-saturated signal obtained at a -40 ppm frequency offset.

Post-Processing of the Lorentzian-Fitted Maps and MTR_{asym} Maps

To compare the Lorentzian-fitted maps and the corresponding MTR_{asym} maps between the two groups, we performed the following steps using Statistical Parametric Mapping version 12 (SPM12) (<http://www.fil.ion.ucl.ac.uk/spm/software/spm12/>). The 3D T1W image and all Lorentzian-fitted and corresponding MTR_{asym} maps were normalized to the dementia standard template. All maps and gray matter volume (GMV) for each participant were

smoothed for voxel-based analyses between the two groups.

Statistical Analyses

Demographic data and clinical outcome scores were compared between the two groups. Ages and K-MMSE scores were compared using Mann-Whitney tests. Sex was analyzed using chi-squared tests. The total intracranial volume (TIV), total gray matter volume (TGMV), total white matter volume (TWMV), and total cerebrospinal fluid volume (TCSFV) were compared using independent *t* tests.

Statistical analyses of the CEST and GMV maps were performed using both voxel-based and region-of-interest (ROI)-based methods. For the voxel-based analysis, two-sample *t* tests were performed to compare the differences of each map between the dementia and non-dementia groups and to select brain areas as ROIs. A significance level of $p = 0.001$ was applied without correcting for multiple comparisons and clusters with at least 30 contiguous voxels. For the ROI-based analysis, atlas-based ROIs were defined using WFU_Pickatlas (<http://fmri.wfubmc.edu/software/PickAtlas>). We selected the anterior cingulate, hippocampus, parahippocampal gyrus, pons, precuneus, and putamen based on the regions that showed significant differences between the two groups in the voxel-based analysis. Information on the selected ROIs is listed in Supplementary Tables 2 and 4. The values of the Lorentzian-fitted maps, MTR_{asym} maps, and GMV were extracted from the selected ROIs. We performed the following analyses using ROI data. First, an independent two-sample test was used to evaluate the differences in values between the two groups. Second, the Pearson correlation coefficient was obtained to analyze the degrees of association between the GMV value or MMSE score and each CEST index for each group. Third, a receiver operating characteristic (ROC) curve analysis was used to evaluate the differentiation between the two groups for each value, including GMV and CEST indices. ROC curve analysis was performed to evaluate the improvement of group classifications by adding GMV with each CEST index value. For the ROI analyses, a *p* value of less than 0.05 was used to determine the significance level. Statistical analysis was performed using MedCalc (MedCalc Software).

RESULTS

Subject Characteristics

Age ($p < 0.001$), MMSE score ($p < 0.001$), TGMV ($p <$

0.001), TWMV ($p < 0.001$), and TCSFV ($p < 0.001$) differed significantly, while sex ($p = 0.190$) and TIV ($p = 0.057$) did not differ significantly between the two groups. The statistical analyses of the subjects' demographic data are summarized in Table 1.

Lorentzian Fitting of Full Z-Spectrum Images with Special Frequency Offset Protons

Supplementary Fig. 2 shows the results of the Lorentzian-fitted Z-spectrum graphs for each proton pool and the corresponding MTR_{asym} map at the left hippocampus obtained from a participant without dementia (68-years-old/female). Figure 1 shows the representative maps of magnitude, amide, amine, OH, direct water saturation, magnetization transfer (MT), and NOE protons after Lorentzian fitting and the MTR_{asym} maps at 1.0, 2.0, 3.0, and 3.5 ppm for participants without dementia (Fig. 1A, 65-year-old female) and with dementia (Fig. 1B, 81-years-old female). The fitting percentage error between the acquired Z-spectrum and Lorentzian-fit curves was 0.48%. The coefficient of variation was 1.235% (95% confidence interval [CI]: 0.942–1.528) and the limits of agreement were -0.0043 (95% CI: -0.0055– -0.0031) for the lower limit and 0.0037 (95% CI: 0.0025–0.0049) for the upper limit. For participants without dementia, the amide signal was relatively higher than the amine and OH signals. In participants with dementia, the amide, amine, and OH signals were higher than those of participants without dementia. The MTR_{asym} values in the participants with dementia were also higher than those in the participants without dementia.

Results of Voxel-Based Analyses of CEST Maps and GMV

Figure 2 shows the results of the voxel-based analyses of the Lorentzian-fitted and corresponding MTR_{asym} maps between the two subject groups. For the maps obtained from the Lorentzian fitting (Supplementary Table 2, Supplementary Fig. 3), amide did not differ significantly between the two groups. Amine and OH signals in participants with dementia were significantly higher than those in participants without dementia. Compared to participants without dementia, those with dementia had higher MTR_{asym} values at 2.0, 3.0, and 3.5 ppm and lower MTR_{asym} values at 1.0 ppm (Supplementary Table 3, Supplementary Fig. 4). As expected, the GMV values were higher in participants without dementia than in those with dementia (Supplementary Table 4, Supplementary Fig. 4).

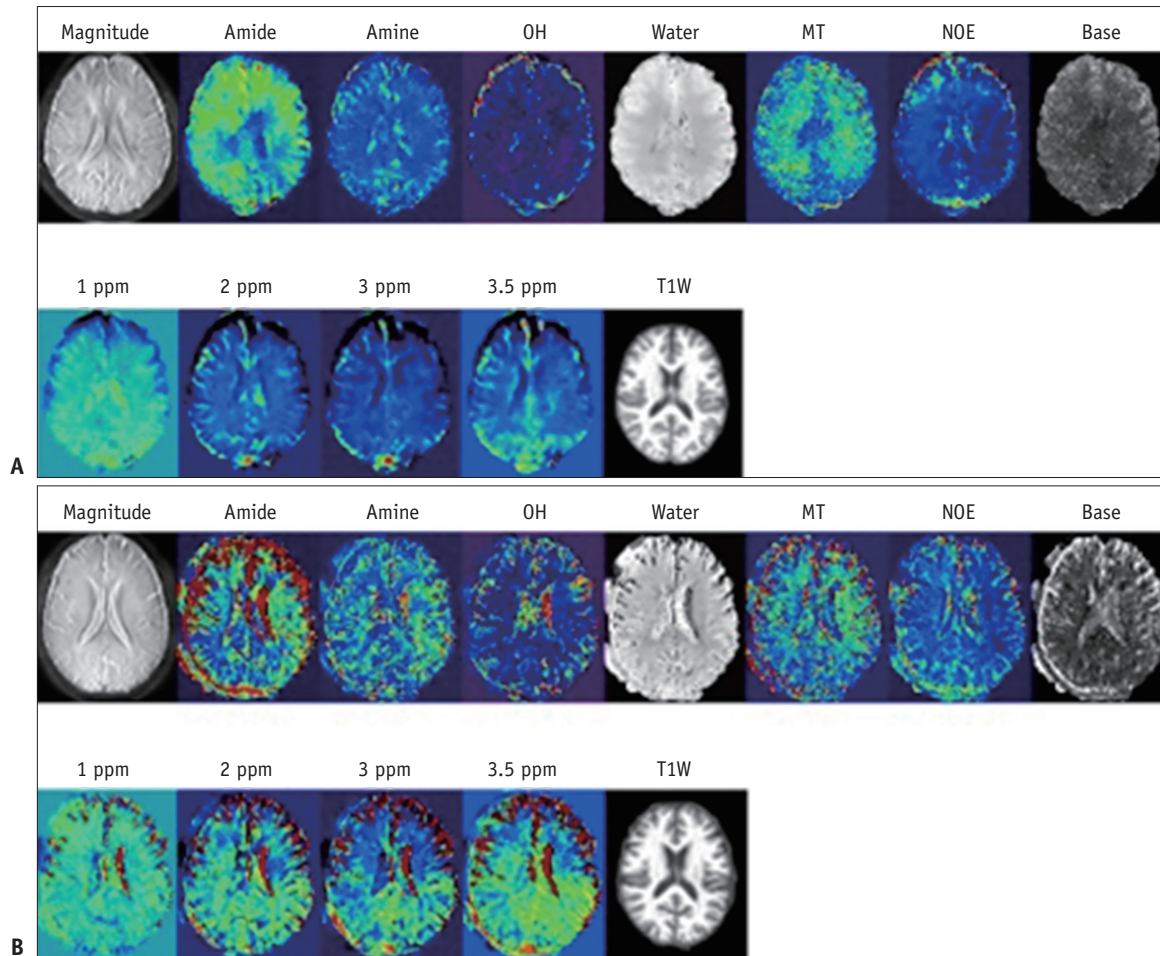


Fig. 1. Representative maps of chemical exchange-dependent saturation transfer signals for participants without dementia (A) and with dementia (B). This figure shows the representative maps of magnitude, amide, amine, OH, direct water saturation (or water), MT, and NOE protons after Lorentzian fitting and MTR_{asym} maps at 1.0, 2.0, 3.0, and 3.5 ppm for participants without dementia (A, 65-year-old female) and with dementia (B, 81-year-old female). MT = magnetization transfer, MTR_{asym} = magnetization transfer ratio asymmetry, NOE = nuclear overhauser effect, OH = hydroxyl, T1W = T1-weighted

Results of ROI-Based Analyses of CEST Maps and GMV

Independent Two-Sample Tests

The mean values with standard deviations are summarized in Table 2 for the Lorentzian-fitted maps of amide, amine, OH, water (direct water saturation [DWS]), MT, and NOE; in Table 3 for the MTR_{asym} maps at 1, 2, 3, and 3.5 ppm; and in Table 4 for GMV. For the Lorentzian-fitted maps (Table 2), the fitted amplitude of water was similar to that of its initial value. The fitted amplitudes of both amide and amine were lower than those of the initial values. The fitted amplitude of OH was greater than its initial value. The fitted amplitude of NOE was similar to that of its initial value. The fitted amplitude of MT was greater than its initial value. Amide levels did not differ significantly between the two groups. Amine (0.029 for non-dementia,

0.046 for dementia, $p = 0.011$ at hippocampus) and OH (0.033 for non-dementia, 0.052 for dementia, $p = 0.019$ at hippocampus) signals were significantly higher in the dementia group than those in the non-dementia group. Water (0.535 for non-dementia, 0.498 for dementia, $p = 0.019$ at hippocampus) and MT (0.205 for non-dementia, 0.179 for dementia, $p = 0.023$ at hippocampus) were significantly lower in the dementia group than those in the non-dementia group. For the MTR_{asym} maps (Table 3), the MTR_{asym} values at 3 ppm (0.748 for non-dementia, 1.138 for dementia, $p = 0.022$ at hippocampus) and 3.5 ppm (0.463 for non-dementia, 0.875 for dementia, $p = 0.029$ at hippocampus) were significantly higher in the dementia group. The MTR_{asym} value at 1 ppm did not differ significantly between the two groups. Finally, the GMV values were significantly higher in the non-dementia group

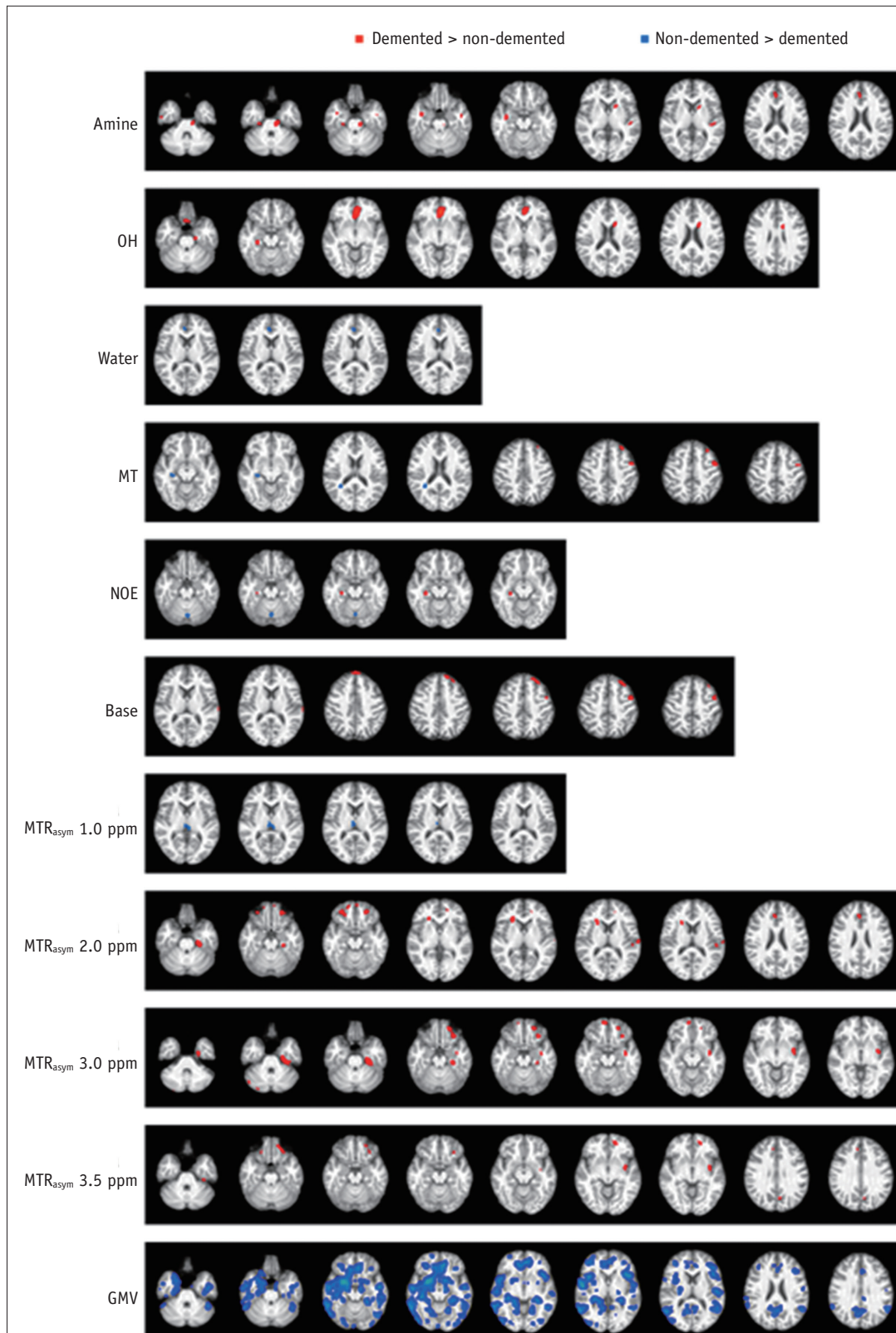


Fig. 2. Results of voxel-based analysis of Lorentzian-fitted maps and MTR_{asym} maps. This figure shows results of voxel-based analysis of Lorentzian-fitted maps of amide, OH, direct water saturation (or water), MT, NOE, and base and MTR_{asym} maps of 1.0, 2.0, 3.0, and 3.5 ppm and GMV. The red color indicates greater measures in the participant with dementia compared to those in the participant without dementia while the blue color indicates the opposite. GMV = gray matter volume, MT = magnetization transfer, MTR_{asym} = magnetization transfer ratio asymmetry, NOE = nuclear overhauser effect, OH = hydroxyl

Table 2. The Lorentzian Map Values of the CEST Data and the Corresponding Results of the Statistical Comparisons between the Participants with and without Dementia for Each ROI

ROI	Non-Dementia (Mean ± SD)	Dementia (Mean ± SD)	P
Amide			
AC	0.037 ± 0.010	0.041 ± 0.022	0.392
Hippocampus	0.022 ± 0.007	0.023 ± 0.009	0.783
Parahippo	0.025 ± 0.010	0.023 ± 0.008	0.405
Pons	0.026 ± 0.009	0.023 ± 0.009	0.195
Precuneus	0.036 ± 0.020	0.029 ± 0.013	0.192
Putamen	0.026 ± 0.009	0.026 ± 0.011	0.821
Amine			
AC	0.041 ± 0.007	0.048 ± 0.010	0.025*
Hippocampus	0.029 ± 0.007	0.046 ± 0.029	0.011*
Parahippo	0.033 ± 0.008	0.049 ± 0.030	0.018*
Pons	0.035 ± 0.010	0.053 ± 0.028	0.009*
Precuneus	0.039 ± 0.015	0.040 ± 0.014	0.987
Putamen	0.034 ± 0.008	0.044 ± 0.021	0.051
OH			
AC	0.043 ± 0.014	0.066 ± 0.030	0.003*
Hippocampus	0.033 ± 0.014	0.052 ± 0.032	0.019*
Parahippo	0.042 ± 0.015	0.058 ± 0.034	0.046*
Pons	0.066 ± 0.023	0.075 ± 0.029	0.268
Precuneus	0.049 ± 0.028	0.047 ± 0.029	0.781
Putamen	0.025 ± 0.010	0.035 ± 0.024	0.079
Water			
AC	0.574 ± 0.046	0.525 ± 0.057	0.004*
Hippocampus	0.535 ± 0.041	0.498 ± 0.058	0.019*
Parahippo	0.537 ± 0.040	0.502 ± 0.058	0.032*
Pons	0.455 ± 0.102	0.448 ± 0.078	0.808
Precuneus	0.502 ± 0.052	0.492 ± 0.053	0.559
Putamen	0.538 ± 0.045	0.505 ± 0.062	0.053
MT			
AC	0.266 ± 0.052	0.255 ± 0.059	0.558
Hippocampus	0.205 ± 0.039	0.179 ± 0.032	0.024*
Parahippo	0.198 ± 0.033	0.179 ± 0.021	0.039*
Pons	0.186 ± 0.046	0.190 ± 0.037	0.776
Precuneus	0.200 ± 0.049	0.195 ± 0.046	0.767
Putamen	0.235 ± 0.036	0.201 ± 0.056	0.024*
NOE			
AC	0.017 ± 0.006	0.020 ± 0.010	0.201
Hippocampus	0.013 ± 0.005	0.017 ± 0.008	0.038*
Parahippo	0.015 ± 0.006	0.019 ± 0.009	0.064
Pons	0.018 ± 0.009	0.019 ± 0.005	0.797
Precuneus	0.018 ± 0.013	0.016 ± 0.008	0.556
Putamen	0.010 ± 0.005	0.013 ± 0.006	0.103
Base			
AC	0.899 ± 0.088	0.853 ± 0.106	0.133
Hippocampus	0.782 ± 0.051	0.734 ± 0.066	0.147
Parahippo	0.782 ± 0.048	0.738 ± 0.063	0.016*
Pons	0.699 ± 0.148	0.697 ± 0.105	0.968
Precuneus	0.769 ± 0.090	0.751 ± 0.088	0.539
Putamen	0.811 ± 0.062	0.748 ± 0.094	0.494

The maximum value is one, indicating 100%. Data show mean ± SD. *Statistical significant difference between the two groups. AC = anterior cingulate, Amide = amide proton group centered at 3.5 ppm, Amine = amine proton group centered at 3.0 ppm, CEST = chemical exchange saturation transfer, DWS = direct water saturation, MT = magnetization transfer at -1.5 ppm, NOE = nuclear overhauser effect centered at -3.5 ppm, OH = hydroxyl proton group centered at 0.9 ppm, Parahippo = parahippocampal gyrus, ROI = region-of-interest, Water = DWS at 0 ppm

Table 3. The MTR_{asym} Values at 1, 2, 3, and 3.5 ppm Offset Frequencies and the Corresponding Results of the Statistical Comparisons between the Participants with and without Dementia for Each ROI

ROI	Non-Dementia (Mean ± SD)	Dementia (Mean ± SD)	P
1 ppm			
AC	-0.243 ± 0.508	0.095 ± 0.686	0.078
Hippocampus	0.232 ± 0.138	0.165 ± 0.178	0.186
Parahippo	0.245 ± 0.137	0.174 ± 0.175	0.153
Pons	0.322 ± 0.215	0.418 ± 0.238	0.179
Precuneus	0.250 ± 0.398	0.202 ± 0.374	0.696
Putamen	0.243 ± 0.139	0.306 ± 0.304	0.382
2 ppm			
AC	0.543 ± 0.548	1.097 ± 0.939	0.024*
Hippocampus	0.887 ± 0.287	1.190 ± 0.658	0.057
Parahippo	0.991 ± 0.347	1.225 ± 0.494	0.084
Pons	0.892 ± 0.514	1.234 ± 0.652	0.068
Precuneus	0.935 ± 0.771	1.158 ± 0.825	0.377
Putamen	1.116 ± 0.308	1.190 ± 0.658	0.064
3 ppm			
AC	0.290 ± 0.662	0.987 ± 1.269	0.030*
Hippocampus	0.748 ± 0.413	1.138 ± 0.624	0.022*
Parahippo	0.886 ± 0.401	1.163 ± 0.542	0.068
Pons	0.976 ± 0.651	1.172 ± 0.718	0.363
Precuneus	1.070 ± 0.752	1.201 ± 0.839	0.601
Putamen	0.903 ± 0.444	1.230 ± 0.554	0.042*
3.5 ppm			
AC	-0.090 ± 0.678	0.954 ± 1.469	0.005*
Hippocampus	0.463 ± 0.374	0.875 ± 0.754	0.029*
Parahippo	0.635 ± 0.436	0.831 ± 0.712	0.288
Pons	0.812 ± 0.745	0.857 ± 0.863	0.861
Precuneus	0.904 ± 0.986	1.121 ± 0.866	0.463
Putamen	0.509 ± 0.465	0.985 ± 0.653	0.010*

The unit of this value is percent (%). Data show mean ± SD. *Statistical significant difference between the two groups. AC = anterior cingulate, MTR_{asym} = magnetization transfer ratio asymmetry, Parahippo = parahippocampal gyrus, ROI = region-of-interest

Table 4. Results of the Statistical Comparisons of the GMV Values between the Participants with and without Dementia for Each ROI and Results of ROC Curve Analysis of GMV in Each ROI for the Group Classification

ROI	Non-Dementia (Mean ± SD)	Dementia (Mean ± SD)	P	AUC	P
Anterior cingulate	0.342 ± 0.036	0.266 ± 0.029	< 0.0001	0.938	< 0.001
Hippocampus	0.483 ± 0.054	0.350 ± 0.064	< 0.0001	0.955	< 0.001
Parahippocampal gyrus	0.451 ± 0.047	0.345 ± 0.046	< 0.0001	0.957	< 0.001
Pons	0.035 ± 0.004	0.031 ± 0.005	0.0074	0.733	0.004
Precuneus	0.324 ± 0.036	0.271 ± 0.032	< 0.0001	0.879	< 0.001
Putamen	0.400 ± 0.039	0.358 ± 0.039	0.0012	0.780	< 0.001

The maximum value is one, which is 100%. Data are presented as mean ± SD. AC = anterior cingulate, AUC = area under the ROC curve, GMV = gray matter volume, ROC = receiver operating characteristic

than those in the dementia group for all ROIs (Table 4).

Correlation Analyses between the GMV and MMSE Scores and Each CEST Index

Correlation with GMV

Amide, OH, MT, Base, and MTR_{asym} at 2 ppm were not significantly correlated with GMV for all ROIs and for both participant groups. In the dementia group, GMV was significantly correlated with amine levels. For the non-dementia group, GMV was significantly correlated with MTR_{asym} (Supplementary Table 5, Supplementary Fig. 5A).

Correlation with MMSE Score

Amide and MTR_{asym} at 1, 2, and 3 ppm were not significantly correlated with the MMSE score for all ROIs. The MMSE score was significantly correlated with amine, OH, DWS, NOE, and base. In addition, the MMSE score was significantly correlated only with MTR_{asym} at 3.5 ppm. Finally, the MMSE score was significantly correlated with GMV in all ROIs (Supplementary Table 5, Supplementary Fig. 5B).

ROC Curve Analyses

A significant difference between the two groups was seen in amine, OH, DWS, MT, NOE, base, and MTR_{asym} at 2, 3, and 3.5 ppm. The amide signal and MTR_{asym} value at 1 ppm did not differ significantly in both participant groups. The participant groups were significantly differentiated by GMV. GMV had larger area under the ROC curve (AUC) values than those for the CEST indices (Supplementary Table 6, Supplementary Fig. 6).

Evaluation of CEST Index Added Value with GMV

The addition of the CEST index slightly improved the classification between the participant groups. The largest improvement was seen in the MTR_{asym} at 2 ppm in the

anterior cingulate (AUC = 0.981). The second-largest improvement was seen for both the DWS and base. Other indices showing slight improvement were amide, OH, DWS, MT, base, and MTR_{asym} at 1, 2, 3, and 3.5 ppm. The results are summarized in Table 5.

DISCUSSION

CEST Signals in AD

The amine signal was higher in the dementia group than that in the non-dementia group (Table 2). The amine signals in the selected ROIs were approximately 4.0–5.3% in the dementia group, compared to 2.9–4.1% in the non-dementia group, indicating that the amine signal may be dominant in subjects with dementia. Our study did not show any significant difference in amide signal between the two groups. In the AD brain, the concentration of proteins and the pH are increased. Both factors can lead to alteration in the signals of exchangeable protons. Several studies have investigated protein imaging using CEST [6, 21, 22]. Although our study showed the usefulness of the multi-pool quantification of a full CEST spectrum using six-pool Lorentzian fitting, post-processing with Lorentzian fitting is complicated and the processing time is too long. Therefore, a simple processing tool with a short running time should be developed for use in routine clinics.

Our results showed that the MTR_{asym} value at 3.0 ppm in the hippocampus was higher in participants with dementia than that in participants without dementia (Table 3). The MTR_{asym} value at 3.0 ppm in the hippocampus was 1.138% in participants with dementia, compared to 0.748% in participants without dementia. This result differed from that of a previous study [8] because the previous study was performed using amide proton transfer (APT) rather than full-spectrum CEST. This is the first study to investigate amine signals in participants with dementia. A previous APT study showed a higher MTR_{asym} value at 3.5 ppm in the hippocampus in the AD group than that in the normal controls [8], as was also observed in the present study.

The possible contributions to the CEST signal changes, including the MTR_{asym} , in the AD brain condition include amide signal changes due to increasing concentrations of A β [6, 21] and/or tau [23] peptides, amine signal changes with increasing peptides [6, 21, 23], increased acidity [2], decreased glutamate neurotransmitters at 3 ppm [24] and OH signal changes at approximately 1 ppm due to increased myo-inositol [25]. A previous study reported insoluble

Table 5. Results of the ROC Curve Analysis to Evaluate the Added Values of CEST Indices with GMV for the Group Classifications

ROI	AUC	<i>P</i>	Combined AUC	<i>P</i>
Amide				
AC	0.505	0.960	0.950	< 0.001
Hippocampus	0.526	0.788	0.964	< 0.001
Parahippo	0.514	0.882	0.959	< 0.001
Pons	0.577	0.405	0.770	0.006
Precuneus	0.567	0.472	0.888	< 0.001
Putamen	0.522	0.821	0.778	0.002
Amine				
AC	0.707	0.018	0.940	< 0.001
Hippocampus	0.700	0.028	0.955	< 0.001
Parahippo	0.718	0.019	0.959	< 0.001
Pons	0.737	0.004	0.801	0.001
Precuneus	0.544	0.636	0.888	< 0.001
Putamen	0.627	0.183	0.825	< 0.001
OH				
AC	0.717	0.010	0.967	< 0.001
Hippocampus	0.679	0.049	0.955	< 0.001
Parahippo	0.648	0.121	0.959	< 0.001
Pons	0.541	0.668	0.744	0.003
Precuneus	0.525	0.796	0.876	< 0.001
Putamen	0.586	0.368	0.811	< 0.001
Water DWS				
AC	0.756	< 0.001	0.976	< 0.001
Hippocampus	0.696	0.023	0.967	< 0.001
Parahippo	0.684	0.032	0.969	< 0.001
Pons	0.556	0.540	0.730	0.005
Precuneus	0.533	0.717	0.885	< 0.001
Putamen	0.645	0.113	0.833	< 0.001
MT				
AC	0.522	0.818	0.964	< 0.001
Hippocampus	0.678	0.036	0.959	< 0.001
Parahippo	0.678	0.035	0.962	< 0.001
Pons	0.525	0.787	0.737	0.003
Precuneus	0.507	0.939	0.880	< 0.001
Putamen	0.638	0.122	0.842	< 0.001
NOE				
AC	0.575	0.409	0.945	< 0.001
Hippocampus	0.681	0.035	0.952	< 0.001
Parahippo	0.669	0.056	0.955	< 0.001
Pons	0.563	0.488	0.739	0.003
Precuneus	0.537	0.692	0.892	< 0.001
Putamen	0.657	0.074	0.830	< 0.001
Base				
AC	0.627	0.161	0.967	< 0.001
Hippocampus	0.697	0.018	0.957	< 0.001
Parahippo	0.695	0.019	0.976	< 0.001
Pons	0.547	0.614	0.737	0.003
Precuneus	0.554	0.561	0.892	< 0.001
Putamen	0.689	0.026	0.837	< 0.001

Table 5. Results of the ROC Curve Analysis to Evaluate the Added Values of CEST Indices with GMV for the Group Classifications (Continued)

ROI	AUC	P	Combined AUC	P
MTR_{asym} 1 ppm				
AC	0.632	0.1421	0.967	< 0.001
Hippocampus	0.617	0.2037	0.959	< 0.001
Parahippo	0.629	0.1540	0.959	< 0.001
Pons	0.644	0.1142	0.794	< 0.001
Precuneus	0.536	0.6992	0.876	< 0.001
Putamen	0.524	0.8052	0.799	< 0.001
MTR_{asym} 2 ppm				
AC	0.682	0.034	0.981	< 0.001
Hippocampus	0.656	0.096	0.955	< 0.001
Parahippo	0.612	0.220	0.962	< 0.001
Pons	0.642	0.106	0.780	< 0.001
Precuneus	0.620	0.194	0.880	< 0.001
Putamen	0.683	0.045	0.852	< 0.001
MTR_{asym} 3 ppm				
AC	0.667	0.055	0.957	< 0.001
Hippocampus	0.708	0.015	0.957	< 0.001
Parahippo	0.658	0.073	0.969	< 0.001
Pons	0.593	0.327	0.792	0.001
Precuneus	0.586	0.355	0.880	< 0.001
Putamen	0.677	0.040	0.821	< 0.001
MTR_{asym} 3.5 ppm				
AC	0.760	< 0.001	0.962	< 0.001
Hippocampus	0.672	0.059	0.959	< 0.001
Parahippo	0.586	0.372	0.964	< 0.001
Pons	0.557	0.547	0.734	0.004
Precuneus	0.605	0.250	0.888	< 0.001
Putamen	0.703	0.014	0.825	< 0.001

Combined AUC, AUC value by both CEST index and GMV. AC = anterior cingulate, AUC = area under the ROC curve, CEST = chemical exchange saturation transfer, DWS = direct water saturation, GMV = gray matter volume, MT = magnetization transfer, MTR_{asym} = magnetization transfer ratio asymmetry, NOE = nuclear overhauser effect, OH = hydroxyl, Parahippo = parahippocampal gyrus, ROC = receiver operating characteristic, ROI = region-of-interest

Aβ₄₂ protein levels of 8.3 μg/g in a normal subject and 117.3 μg/g in a patient with AD [26]. In general, amyloid deposition in AD starts in the cortex and spreads to other parts of the brain [27]. The amines in the amino acids become amides when they form Aβ peptides and the amines in the side chain of the amino acid residues, such as lysine, aspartic acid, glutamine, and histidine, are retained as amines. Many exchangeable protons differ between the oligomers and plaques of Aβ peptides [6]; therefore, protein aggregation [21] and the progression of protein misfolding

[22] may be mapped. The pH is approximately 7.0 in the brain of a normal healthy subject [28] and approximately 7.4 in the AD brain [29]. Previous studies have shown that amide is sensitive to changes in protein concentrations, while amine is sensitive to changes in pH [2, 3]. Therefore, future studies are needed to compare CEST signals to amyloid PET and/or tau PET in participants with AD. Furthermore, further studies are warranted to compare CEST signals to metabolite signals using MR spectroscopy in the AD brain.

CEST Signals Correlated with MMSE Scores and GMV

The amine signal was significantly negatively correlated with MMSE scores, indicating that amine is lower in normal controls than in participants with dementia. While the amide signal was negatively correlated with MMSE scores, the relationship was not statistically significant. A previous APT study showed that MTR_{asym} values at a 3.5 ppm offset in the hippocampus were negatively correlated with MMSE scores [8]. Most CEST indices were not significantly correlated with GMV in either the non-dementia and dementia groups, indicating that CEST signal changes did not directly represent a neuronal loss in the brain and independently measure alterations in the brain. Therefore, CEST signals may be affected by other factors such as alterations of metabolites and/or distributions of proteins in the brain.

Added Value of the CEST Index with GMV for Group Classification

GMV had larger AUC values than those of the CEST indices. GMV had good group differentiation with good sensitivity and specificity. However, the CEST indices had relatively low power for classification, with low sensitivity and specificity. This study evaluated the potential usefulness of CEST imaging as an added technique with GMV for group classification. We found an improvement in the classification between the participant groups using both the CEST index and GMV. The largest improvement was seen in the MTR_{asym} at 2 ppm in the anterior cingulate (AUC = 0.981), with good sensitivity (100) and specificity (90.91). In addition, measurement of the water component in the CEST image, which is represented by DWS, was valuable as an added technique for group classification (AUC = 0.976), with good sensitivity (100) and specificity (90.91). Therefore, the CEST map can be used to provide added value to the GMV to differentiate between participants with and

without dementia. In patients with AD, CEST MRI with atrophy detection can be valuable for the improvement of the group classification of individuals.

In conclusion, this first application of full-frequency CEST data using six-pool Lorentzian fitting showed a higher amine signal and MTR_{asym} value at 3.0 ppm in the hippocampus in the dementia group than those in the non-dementia group, demonstrating AD-related brain changes in participants with dementia as compared to those in participants without dementia. The amine signal, which was lower in participants without dementia than that in participants with dementia, was significantly negatively correlated with MMSE score, indicating that amine could be a potential imaging biomarker to evaluate cognitive decline in AD. Although GMV itself had good group differentiation with good sensitivity and specificity, we observed improved classification between the participant groups using both CEST index and GMV, indicating that the CEST index can be used as an added-value parameter to differentiate between participants. CEST MRI may allow noninvasive identification of image alterations in the AD brain without injecting isotopes for monitoring different disease states and, thus, may be used as a new imaging biomarker in the future. Further studies are needed to compare CEST to amyloid PET and/or metabolite signals by MR spectroscopy.

Supplementary Materials

The Data Supplement is available with this article at <https://doi.org/10.3348/kjr.2020.0700>.

Conflicts of Interest

The authors have no potential conflicts of interest to disclose.

Acknowledgments

We thank Dr. Ha-Kyu Jeong at Samsung Electronics Company for his technical support and valuable advice in the application of the chemical exchange dependent saturation transfer technique and Dr. Jinyuan Zhou at Johns Hopkins University School of Medicine in Baltimore, USA for supporting the CEST sequence and for his fruitful advice. In addition, the authors thank Miss Soo-Jin Kim for providing statistical support.

Author Contributions

Conceptualization: Key Chung Park, Chang-Woo Ryu, Eui

Jong Kim, Geon-Ho Jahng. Data curation: Jang-Hoon Oh, Bo Guem Choi, Geon-Ho Jahng. Formal analysis: Jang-Hoon Oh, Bo Guem Choi, Chang-Woo Ryu, Geon-Ho Jahng. Funding acquisition: Geon-Ho Jahng. Investigation: Hak Young Rhee, Jin San Lee, Kyung Mi Lee, Soonchan Park, Ah Rang Cho, Chang-Woo Ryu, Key Chung Park, Eui Jong Kim, Geon-Ho Jahng. Methodology: Jang-Hoon Oh, Hak Young Rhee, Jin San Lee, Kyung Mi Lee, Soonchan Park, Ah Rang Cho, Chang-Woo Ryu, Key Chung Park, Eui Jong Kim, Geon-Ho Jahng. Project administration: Hak Young Rhee, Geon-Ho Jahng. Resources: Hak Young Rhee, Jin San Lee, Kyung Mi Lee, Soonchan Park, Ah Rang Cho, Chang-Woo Ryu, Key Chung Park, Eui Jong Kim, Geon-Ho Jahng. Software: Jang-Hoon Oh, Bo Guem Choi, Geon-Ho Jahng. Supervision: Key Chung Park, Eui Jong Kim, Geon-Ho Jahng. Validation: Jang-Hoon Oh, Geon-Ho Jahng. Visualization: Jang-Hoon Oh, Bo Guem Choi, Geon-Ho Jahng. Writing—original draft: all authors. Writing—review & editing: all authors.

ORCID iDs

Jang-Hoon Oh

<https://orcid.org/0000-0002-4251-5470>

Bo Guem Choi

<https://orcid.org/0000-0001-9084-3340>

Hak Young Rhee

<https://orcid.org/0000-0002-3016-2591>

Jin San Lee

<https://orcid.org/0000-0002-5017-854X>

Kyung Mi Lee

<https://orcid.org/0000-0003-3424-0208>

Soonchan Park

<https://orcid.org/0000-0001-6057-7117>

Ah Rang Cho

<https://orcid.org/0000-0003-0652-2929>

Chang-Woo Ryu

<https://orcid.org/0000-0002-4674-7295>

Key Chung Park

<https://orcid.org/0000-0001-8250-9561>

Eui Jong Kim

<https://orcid.org/0000-0003-2183-8657>

Geon-Ho Jahng

<https://orcid.org/0000-0001-8881-1884>

REFERENCES

1. Kogan F, Hariharan H, Reddy R. Chemical Exchange Saturation Transfer (CEST) imaging: description of technique and

- potential clinical applications. *Curr Radiol Rep* 2013;1:102-114
2. Zhou J, Payen JF, Wilson DA, Traystman RJ, van Zijl PC. Using the amide proton signals of intracellular proteins and peptides to detect pH effects in MRI. *Nat Med* 2003;9:1085-1090
 3. Oh JH, Kim HG, Woo DC, Jeong HK, Lee SY, Jahng GH. Chemical-exchange-saturation-transfer magnetic resonance imaging to map gamma-aminobutyric acid, glutamate, myoinositol, glycine, and asparagine: phantom experiments. *J Korean Phys Soc* 2017;70:545-553
 4. van Zijl PC, Yadav NN. Chemical exchange saturation transfer (CEST): what is in a name and what isn't? *Magn Reson Med* 2011;65:927-948
 5. Yadav NN, Jones CK, Hua J, Xu J, van Zijl PC. Imaging of endogenous exchangeable proton signals in the human brain using frequency labeled exchange transfer imaging. *Magn Reson Med* 2013;69:966-973
 6. Goerke S, Milde KS, Bukowiecki R, Kunz P, Klika KD, Wiglenda T, et al. Aggregation-induced changes in the chemical exchange saturation transfer (CEST) signals of proteins. *NMR Biomed* 2017 Jan [Epub]. <https://doi.org/10.1002/nbm.3665>
 7. Jahng GH, Choi W, Chung JJ, Kim ST, Rhee HY. Mapping exchangeable protons to monitor protein alterations in the brain of an Alzheimer's disease mouse model by using MRI. *Curr Alzheimer Res* 2018;15:1343-1353
 8. Wang R, Li SY, Chen M, Zhou JY, Peng DT, Zhang C, et al. Amide proton transfer magnetic resonance imaging of Alzheimer's disease at 3.0 Tesla: a preliminary study. *Chin Med J (Engl)* 2015;128:615-619
 9. Zaiss M, Schmitt B, Bachert P. Quantitative separation of CEST effect from magnetization transfer and spillover effects by Lorentzian-line-fit analysis of z-spectra. *J Magn Reson* 2011;211:149-155
 10. Jones CK, Huang A, Xu J, Edden RA, Schär M, Hua J, et al. Nuclear Overhauser enhancement (NOE) imaging in the human brain at 7T. *Neuroimage* 2013;77:114-124
 11. Desmond KL, Moosvi F, Staniszc GJ. Mapping of amide, amine, and aliphatic peaks in the CEST spectra of murine xenografts at 7 T. *Magn Reson Med* 2014;71:1841-1853
 12. Ahn HJ, Chin J, Park A, Lee BH, Suh MK, Seo SW, et al. Seoul Neuropsychological Screening Battery-dementia version (SNSB-D): a useful tool for assessing and monitoring cognitive impairments in dementia patients. *J Korean Med Sci* 2010;25:1071-1076
 13. McKhann G, Drachman D, Folstein M, Katzman R, Price D, Stadlan EM. Clinical diagnosis of Alzheimer's disease: report of the NINCDS-ADRDA Work Group under the auspices of Department of Health and Human Services Task Force on Alzheimer's Disease. *Neurology* 1984;34:939-944
 14. Petersen RC, Smith GE, Waring SC, Ivnik RJ, Tangalos EG, Kokmen E. Mild cognitive impairment: clinical characterization and outcome. *Arch Neurol* 1999;56:303-308
 15. Petersen RC, Doody R, Kurz A, Mohs RC, Morris JC, Rabins PV, et al. Current concepts in mild cognitive impairment. *Arch Neurol* 2001;58:1985-1992
 16. Zhu H, Jones CK, van Zijl PC, Barker PB, Zhou J. Fast 3D chemical exchange saturation transfer (CEST) imaging of the human brain. *Magn Reson Med* 2010;64:638-644
 17. Zhao X, Wen Z, Huang F, Lu S, Wang X, Hu S, et al. Saturation power dependence of amide proton transfer image contrasts in human brain tumors and strokes at 3 T. *Magn Reson Med* 2011;66:1033-1041
 18. Jahng GH, Oh JH. Physical modeling of chemical exchange saturation transfer imaging. *Prog Med Phys* 2017;28:135-143
 19. Holmes HE, Colgan N, Ismail O, Ma D, Powell NM, O'Callaghan JM, et al. Imaging the accumulation and suppression of tau pathology using multiparametric MRI. *Neurobiol Aging* 2016;39:184-194
 20. Zhou J, Blakeley JO, Hua J, Kim M, Lartera J, Pomper MG, et al. Practical data acquisition method for human brain tumor amide proton transfer (APT) imaging. *Magn Reson Med* 2008;60:842-849
 21. Chen L, Wei Z, Chan KKY, Cai S, Liu G, Lu H, et al. Protein aggregation linked to Alzheimer's disease revealed by saturation transfer MRI. *Neuroimage* 2019;188:380-390
 22. Goerke S, Zaiss M, Kunz P, Klika KD, Windschuh JD, Mogk A, et al. Signature of protein unfolding in chemical exchange saturation transfer imaging. *NMR Biomed* 2015;28:906-913
 23. Wells JA, O'Callaghan JM, Holmes HE, Powell NM, Johnson RA, Siow B, et al. In vivo imaging of tau pathology using multiparametric quantitative MRI. *Neuroimage* 2015;111:369-378
 24. Haris M, Nath K, Cai K, Singh A, Crescenzi R, Kogan F, et al. Imaging of glutamate neurotransmitter alterations in Alzheimer's disease. *NMR Biomed* 2013;26:386-391
 25. Haris M, Singh A, Cai K, Nath K, Crescenzi R, Kogan F, et al. MICEST: a potential tool for non-invasive detection of molecular changes in Alzheimer's disease. *J Neurosci Methods* 2013;212:87-93
 26. Lue LF, Kuo YM, Roher AE, Brachova L, Shen Y, Sue L, et al. Soluble amyloid beta peptide concentration as a predictor of synaptic change in Alzheimer's disease. *Am J Pathol* 1999;155:853-862
 27. Hardy J, Allsop D. Amyloid deposition as the central event in the aetiology of Alzheimer's disease. *Trends Pharmacol Sci* 1991;12:383-388
 28. Chu WJ, Hetherington HP, Kuzniecky RJ, Vaughan JT, Twieg DB, Faught RE, et al. Is the intracellular pH different from normal in the epileptic focus of patients with temporal lobe epilepsy? A 31P NMR study. *Neurology* 1996;47:756-760
 29. Mandal PK, Akolkar H, Tripathi M. Mapping of hippocampal pH and neurochemicals from in vivo multi-voxel 31P study in healthy normal young male/female, mild cognitive impairment, and Alzheimer's disease. *J Alzheimers Dis* 2012;31 Suppl 3:S75-S86